University of SALFORD
MANCHESTER

Viscous dissipation and joule heating effects in non-Fourier MHD squeezing flow, heat and mass transfer between Riga plates with thermal radiation : variational parameter method solutions

Shamshuddin, M, Mishra, SR, Beg, OA and Kadir, A

Title	Viscous dissipation and joule heating effects in non-Fourier MHD squeezing flow, heat and mass transfer between Riga plates with thermal radiation : variational parameter method solutions
Authors	Shamshuddin, M, Mishra, SR, Beg, OA and Kadir, A
Publication title	Arabian Journal for Science and Engineering
Publisher	Springer
Type	Article
USIR URL	This version is available at: http://usir.salford.ac.uk/id/eprint/51015/
Published Date	2019

VISCOUS DISSIPATION AND JOULE HEATING EFFECTS IN NON-FOURIER MHD SQUEEZING FLOW, HEAT AND MASS TRANSFER BETWEEN RIGA PLATES WITH THERMAL RADIATION: *VARIATIONAL PARAMETER METHOD SOLUTIONS*

MD. Shamshuddin[1*], S.R. Mishra[2], O. Anwar Bég[3] and A. Kadir[4]

[1]Department of Mathematics, Vaagdevi College of Engineering, Warangal, Telangana State, **India.**
[2]Department of Mathematics, Siksha O Anusandhan University, Bhubaneswar, **India.**
[3,4]Department of Aeronautical and Mechanical Engineering, University of Salford, Manchester, **UK.**
Corresponding author- Email: shammaths@gmail.com

ABSTRACT

A Riga plate is an electromagnetic actuator which comprises of permanent magnets and alternating electrodes placed on a plane surface. The present article investigates the influence of viscous and Joule heating (Ohmic dissipation) in the magnetohydrodynamic squeezing flow, heat and mass transfer between two Riga plates. A non-Fourier (Cattaneo-Christov) heat flux model is employed which generalizes the classical Fourier law to incorporate thermal relaxation time. Via suitable transformations the governing partial differential conservation equations and boundary conditions are non-dimensionalized. The resulting nonlinear ordinary differential boundary value problem is well-posed and is solved analytically by the variational parameter method (VPM). Validation of the solutions is included for the special case of non-dissipative flow. Extensive graphical illustrations are presented for the effects of squeeze parameter, magnetic field parameter, modified Hartmann number, radiative parameter, thermal Biot number, concentration Biot number, Eckert number, length parameter, Schmidt number and chemical reaction parameter on the velocity, temperature and concentration distributions. Additionally, the influence of selected parameters on reduced skin friction, Nusselt number and Sherwood number are tabulated. An error analysis is also included for the VPM solutions. Detailed interpretation of the results is provided. The study is relevant to smart lubrication systems in biomechanical engineering and sensor design.

KEYWORDS: *Squeezing flow, Riga Plate, Magnetic field, Non-Fourier heat transfer, Reactive mass transfer, Thermal radiation, Viscous Dissipation, Joule Heating, Variational Parameter Method (VPM), smart lubrication.*

NOMENCLATURE

a	dimensional constant
b	width of magnets and electrodes
B	dimensionless constant
B_0	applied magnetic field
B_{i1}	Biot number for temperature
B_{i2}	Biot number for concentration
c	concentration of fluid
c_{f1}	concentration of upper plate
c_f	skin friction coefficient
C_h	ambient temperature

C_p	specific heat capacity
D_B	Brownian diffusion coefficient
Ec	Eckert number
h_1	convective heat transfer
h_2	convective mass transfer
j_0	applied current density
k	thermal conductivity
K_c	dimensionless chemical reaction parameter
M^2	Hartmann magnetic body force parameter
M_0	magnetization
m^*	coefficient of mean absorption
Nu_x	local Nusselt number
p	pressure
Pr	Prandtl number
q_r	radiative heat flux (W/m^2)
R	radiation parameter
Re_x	local Reynolds number
Sc	bioconvection Schmidt number
Sh_x	local Sherwood number
t	time (s)
T	temperature (K)
T_{f1}	temperatures of upper plate
u	velocity component in x-direction (m/s)
U_w	stretching velocity
v	velocity component in y-direction (m/s)
v_f	fluid velocity
Z	modified Hartmann number

GREEK SYMBOLS

β	squeezing parameter
β_e	thermal relaxation time
η	dimensionless variable
ρ	fluid density (kg/m^3)
σ	electric conductivity
σ^*	Stefan-Boltzmann constant
μ	dynamic viscosity of squeeze film
γ	characteristic constant parameter
δ	length parameter
Ω_E	temperature difference
λ_E	thermal radiation time
π	component of deformation
ψ	stream function
θ	dimensional less temperature
ϕ	dimensionless concentration

1   INTRODUCTION

Squeeze film flows [1] are characterized by a thin layer of viscous fluid intercalated between approaching plane surfaces in which viscous effects dominate inertial effects (i.e. a low Reynolds number regime). A common assumption is that the plates are infinite in extent so that edge plates may be neglected. Squeezing flows arise in many diverse applications in engineering including smart dampers [2], anti-corrosion lubricants [3], helicopter rotor bearings [4], microsystems [5] and orthopedic tribology [6-8]. For some years, engineers have also explored the use of *smart lubricants* in squeeze films. These feature "intelligent" fluids which respond to an external stimulus such as electrical or magnetic fields. The advantage of electromagnetic lubricants is that they achieve a variable-damping performance and allow designers to fine tune the vibration of machine components. To simulate magnetic squeeze films mathematically the popular approach is magnetohydrodynamic (MHD) viscous flow models. These may be Newtonian or non-Newtonian depending on the lubricant. Wang *et al.* [9] studied the squeezing flow of a magnetized Bingham (viscoplastic) fluid in a damper-rigid rotor system, deriving and solving Reynolds equation to present extensive solutions for flowing velocity, pressure distribution, film force, and the magnetic pull force of the damper.Usha and Sridharan [10] presented closed-form solutions for the magneto-hydrodynamic squeeze flow between two parallel disks with wall suction or injection, observing that with stronger injection the load carrying capacity is enhanced whereas the opposite response is computed with wall suction. Vadher *et al.* [11] investigated theoretically the magnetofluid squeeze film between two conducting rough porous electrically-conducting conical plates, observing that with higher values of magnetization parameter there is a steady elevation in pressure, load carrying capacity and the response time whereas there is an adverse response to transverse surface roughness. Shimpi and Deheri [12] studied the magnetohydrodynamic squeeze film flow between rotating transversely rough porous annular elastically-deforming plates. They found that the magnetic lubricant enhances bearing performance whereas the roughness of the bearing surfaces and deformation decreases load carrying capacity. Usha and Vimala [13] analyzed magnetic gas squeeze film flow between two circular parallel plates (in sinusoidal relative motion) containing a single central air bubble of cylindrical shape are theoretically investigated. They used both numerical and perturbation techniques to derive solutions for the air bubble radius, pressure distribution, and squeeze film force. Zueco and Bég [14] used an electro-thermal solver to simulate the magnetic Newtonian squeeze film flow between co-rotating disks with electromagnetic induction effects. They observed that both dimensionless axial and azimuthal magnetic field components and axial velocity are enhanced with an increase in rotational Reynolds number whereas the azimuthal velocity is reduced. Kumar *et al.* [15] investigated numerically the magnetic squeezed flow and heat transfer in a tangent hyperbolic rheological transport over a sensor surface with variable thermal conductivity, showing that with increasing Weissenberg (non-Newtonian) number temperature is elevated whereas the contrary response is computed with increased squeezed flow index parameter increased. They also noted that higher magnetic field decreases temperatures and accelerates the flow.

In sophisticated sensor designs and magnetic lubrication systems, the Riga plate is often featured. This is a special electromagnetic actuator which comprises a spanwise aligned array of alternating electrodes and permanent magnets and enables precision flow control. The array permits the mobilization of a surface-parallel Lorentz magnetic body force which decreases exponentially in the direction normal to the plate. This device was first studied by Gailitis and Lielausis [16] who introduced the "Grinberg-term" for the wall parallel Lorentz force

due to Riga plate motion and also identified that the key electromagnetic parameter in Riga plate fluid mechanics is the *modified Hartmann number*. This parameter is positive when the Lorentz body force points in the direction of the free stream (aiding flow) and negative when it is opposite to the free stream (opposing flow). In recent years owing to rapid developments in micro-electromagnetic systems there has been a renewed interest in Riga plate fluid dynamics. Ahmad *et al.* [17] analyzed using both numerical and asymptotic methods the mixed convection boundary layer flow of a nanofluid from a vertical Riga plate with wall suction, computing skin friction, Nusselt number and Sherwood number. Anjum [18] analyzed the viscoelastic magnetized flow from a Riga plate with heat source and sink effects. Hayat *et al.* [19] presented homotopy solutions for double-diffusive stratified mixed convection from a Riga plate with thermal radiation, showing that buoyancy ratio and modified Hartmann number induces the opposite effects on wall heat transfer rates.

In electromagnetic fluid dynamics, Joule heating (Ohmic dissipation) arises when the energy of an electric current is converted into heat as it flows through a resistance. In particular when electric current flows through a fluid with finite electrical conductivity, electric energy is converted to heat through resistive losses in the fluid. The heat is generated on the microscale when the conduction electrons transfer energy to the conductor atoms by way of collisions. Joule heating has been studied extensively in recent years in hydromagnetic transport phenomena and has been found to exert significant modifications in momentum, heat and mass diffusion characteristics. Mao *et al.* [20] investigated the influence of Joule heating on the heat transfer in a fully developed channel flow between two parallel thin electrically conducting plates under a transverse magnetic field. El-Amin [21] considered both viscous and Joule heating effects in non-isothermal hydromagnetic convection boundary layer flow from a horizontal cylinder in a permeable material. Bég *et al.* [22] examined computationally the Joule and viscous heating effects on time-dependent Hall magneto-gas dynamic flow in a channel containing a porous medium. Srinivasacharya and Jagadeeshwar [23] analysed numerically the Hall current and Joule heating effects on double-diffusive hydromagnetic convection from an exponentially stretching sheet using the Chebyshev pseudo- spectral method. Further studies considering Joule heating effects include Aurangzaib and Shafie [24] (on reactive transient convection from a stretching surface with cross diffusion), Tripathi *et al.* [25] (on nanofluid electro-osmotic pumping) and Golsefid *et al.* [26] (on electrohydrodynamic heat transfer in rectangular enclosures). Further studies of Joule heating in electromagnetic flows include Shamshuddin *et al.* [27] (on transient chemically reacting magnetic radiative micropolar transport from a tilted surface), Hussain *et al.* [28] (on magnetized viscoelastic nanofluid enrobing flow on an extending cylinder), Bég *et al.* [29] (on non-isothermal Hall magnetic generator flow) and Sucharitha *et al.* [30] (on peristaltic pumping of magnetic nanofluids). Squeezing hydromagnetic flows featuring Joule dissipation have also received some attention. Ahmad *et al.* [31] used a homotopy method to study the combined effects of viscous and Joule dissipation and homogeneous-heterogeneous reactions on heat and mass transfer in squeezing flow of a magnetic fluid. They computed the variation in Nusselt number and skin friction. Ghadikolaei *et al.* [32] presented analytical solutions for time-dependent hydromagnetic squeezing flow, heat and mass transfer in an electrically-conducting Eyring-Powell fluid through a stretching channel with Joule heating and radiative flux.

In the current study, the *collective influence of viscous and Joule heating (Ohmic dissipation) in magnetohydrodynamic squeezing flow and heat transfer between two Riga plates* is investigated theoretically. A non-Fourier (Cattaneo-Christov) [33] heat flux model is employed which generalizes the classical Fourier law to incorporate thermal relaxation time. This model has been recently applied successfully in a variety of squeezing

flow lubrication studies including Hayat *et al.* [34] (on chemical reacting squeeze films between Riga plates), Muhammad *et al.* [35] (nanofluid squeezing flows) and Atlas *et al.* [36] (second law thermodynamic analysis of Riga plate squeezing flow). Other recent studies featuring the non-Fourier (Cattaneo-Christov) heat flux model include Von Karman swirling heat transfer as studied by Mishra *et al.* [37] and reactive hydromagnetic viscoelastic non-orthogonal stagnation flow as examined by Mehmood *et al.* [38]. In the present study, following the implementation of a set of transformations, the non-dimensional emerging nonlinear ordinary differential boundary value problem is solved analytically by the variational parameter method (VPM) introduced by Ma *et al.* [39]. Validation of the solutions is included for the special case of non-dissipative flow. The influence of squeeze parameter, magnetic field parameter, modified Hartmann number, radiative parameter, thermal Biot number, concentration Biot number, Eckert number, length parameter, Schmidt number and chemical reaction parameter on the velocity, temperature and concentration distributions is visualized graphically. The influence of selected parameters on reduced skin friction, Nusselt number and Sherwood number is also tabulated. An error analysis is also included for the VPM solutions. Extensive interpretation of the results is provided. The current problem Previous studies have *neglected viscous and Joule dissipation effects*. These are important in real magnetic lubrication systems since they capture actual thermal dissipation effects via fluid friction and electromagnetic field and provide a more accurate appraisal of the efficiency of such systems. The current study therefore incorporates these effects in conjunction with non-Fourier heat transfer and chemical reactivity of the working fluid, and thereby provides a more generalized model for Riga plate transport phenomena. The model described therefore, to the authors' knowledge, not yet received attention in the literature and constitutes an important extension to the existing body of work. The results have important potential applications in disk type magnetic clutches in automobile engineering [40], electromagnetic squeeze-film pressure sensor systems in micro-biomedical systems [41] and magnetic sensor lubrication flows in materials processing [42, 43]. Furthermore, this work is the first to apply the VPM technique to electromagnetic Riga plate lubrication flows and therefore provides researchers with alternative numerical approaches to those traditionally used in tribology simulations.

2 ELECTROMAGNETIC DUAL RIGA PLATE SQUEEZE FILM MODEL

We consider the two-dimensional time-dependent electromagnetic squeezing viscous flow between two parallel Riga plates, as depicted in **Fig. 1**. The upper Riga plate is located at $y = h(t) = \sqrt{v_f (1 - \gamma t)/a}$ and the lower Riga plate (positioned at $y = 0$) is capable of stretching in its own plane with velocity $U_w = ax(1 - \gamma t)^{-1}$. The upper rigid (non-deformable) Riga plate approaches towards the lower stretching Riga plate and this approach motion generates an electromagnetic squeezing film flow with velocity $v_h = dh/dt$. Heat transfer occurs in the flow regime and due to the presence of thermal relaxation, the *Cattaneo-Christov non-Fourier heat flux model* is deployed. The intercalated Newtonian lubricant is doped with a reactive species and mass diffusion is also present which obeys the Fickian law. An aligned magnetic field is applied parallel to the Riga plates. Thermal radiation flux is also present as are viscous dissipation and Joule heating (Ohmic dissipation) effects. Isothermal and iso-solutal conditions are enforced at both Riga plates. A Cartesian coordinate system (x, y) is adopted as shown in **Fig. 1**. The appropriate mass, primary and secondary momentum, energy and species (concentration) conservation

equations describing the transport phenomena in the squeeze film regime are an amalgamation of the model for chemically-reacting Riga plate flow used by Hayat *et al.* [34] with supplementary terms for viscous and Joule heating following Mao *et al.* [20], El-Amin [21] and Bég *et al.* [22] combined with the non-Fourier heat transfer model of Muhammad *et al.* [35] and take the form:
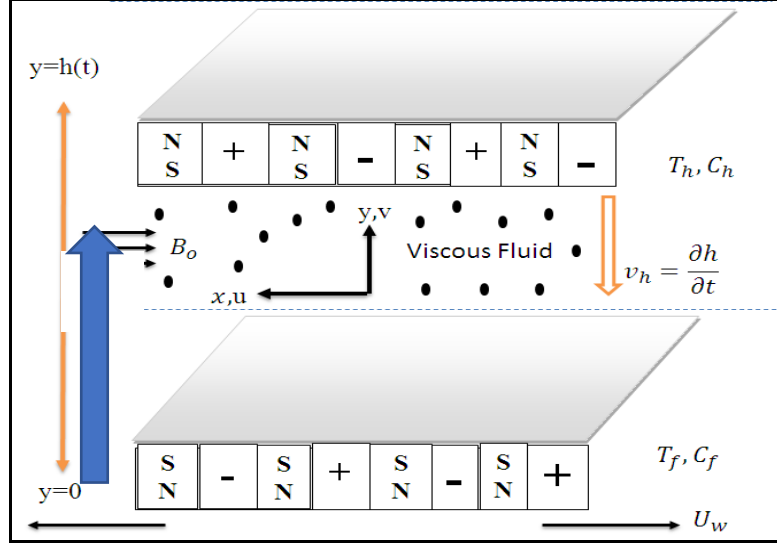

Fig 1: Physical description of the dual Riga plate squeezing flow problem

$$\frac{\partial u}{\partial x} + \frac{\partial v}{\partial y} = 0, \tag{1}$$

$$\frac{\partial u}{\partial t} + u\frac{\partial u}{\partial x} + v\frac{\partial u}{\partial y} = -\frac{1}{\rho_f}\frac{\partial p}{\partial x} + v_f\left(\frac{\partial^2 u}{\partial x^2} + \frac{\partial^2 u}{\partial y^2}\right) - \frac{\sigma B_0^2}{\rho(1-\gamma t)}u + \frac{\pi j_0 M_0}{8\rho_f}Exp\left(-\frac{\pi}{b}y\right), \tag{2}$$

$$\frac{\partial v}{\partial t} + u\frac{\partial v}{\partial x} + v\frac{\partial v}{\partial y} = -\frac{1}{\rho_f}\frac{\partial p}{\partial y} + v_f\left(\frac{\partial^2 v}{\partial x^2} + \frac{\partial^2 v}{\partial y^2}\right), \tag{3}$$

$$\frac{\partial T}{\partial t} + u\frac{\partial T}{\partial x} + v\frac{\partial T}{\partial y} + \lambda_E\Omega_E = \frac{k_f}{(\rho cp)_f}\left(\frac{\partial^2 T}{\partial x^2} + \frac{\partial^2 T}{\partial y^2}\right) - \frac{1}{(\rho cp)_f}\frac{\partial q_r}{\partial y} + \frac{\mu}{\rho cp}\left[4\left(\frac{\partial u}{\partial x}\right)^2 + \left(\frac{\partial u}{\partial y} + \frac{\partial v}{\partial x}\right)^2\right]$$
$$+ \frac{\sigma B_0^2}{\rho cp(1-\gamma t)}u^2 \tag{4}$$

$$\frac{\partial C}{\partial t} + u\frac{\partial C}{\partial x} + v\frac{\partial C}{\partial y} = D_B\left(\frac{\partial^2 C}{\partial x^2} + \frac{\partial^2 C}{\partial y^2}\right) - K_1(C - C_h). \tag{5}$$

The following boundary conditions are enforced at the lower Riga plate and upper Riga plate, respectively:

$$at \ \ y = 0: \ \ \ u = U_w = \frac{ax}{(1-\gamma t)}, \ v = 0, \ \frac{\partial T}{\partial y} = -\frac{h_1}{k}\left(T_{f1} - T\right), \ \frac{\partial C}{\partial y} = -\frac{h_2}{D}\left(C_{f1} - C\right)$$

$$at \ \ y = h(t): \ u = 0, \ v = v_h = \frac{dh}{dt} = -\frac{\gamma}{2}\sqrt{v/a(1-\gamma t)}, \ T = T_h, \ C = C_h \tag{6}$$

Here U_w represents the stretching velocity, a represents dimensional constant, h_1 represents convective heat transfer, h_2 represents convective mass transfer, T_{f1} represents temperature of upper plate, C_{f1} represents concentration of upper plate also the boundary conditions describes that lower plate is placed at $y = 0$ and stretched in the x-direction with the plate velocity U_w and in y-direction with the velocity $v = 0$ as described in [33]. The convective boundary conditions describe the energy balance at the fluid-solid interface. The Dirichlet boundary conditions are used for both temperature and concentration at the upper plate. The Rosseland diffusion flux approximation is employed which is appropriate for optically-thick fluids. The appropriate expression for the radiative heat flux q_r is [44]:

$$q_r = \frac{4\sigma^*}{3m^*} \frac{\partial\left(T^4\right)}{\partial y} = -\frac{16\sigma^*}{3m^*} T^3 \frac{\partial T}{\partial y} \quad , \tag{7}$$

Invoking Eqn. (7) in Eqn. (4), the energy equation is converted to the following:

$$\frac{\partial T}{\partial t} + u\frac{\partial T}{\partial x} + v\frac{\partial T}{\partial y} + \lambda_E \Omega_E = \frac{k_f}{(\rho cp)_f}\left(\frac{\partial^2 T}{\partial x^2} + \frac{\partial^2 T}{\partial y^2}\right) + \frac{1}{(\rho cp)_f}\frac{\partial}{\partial y}\left(\frac{16\sigma^*}{3m^*}T^3\frac{\partial T}{\partial y}\right)$$
$$+ \frac{\mu}{\rho cp}\left[4\left(\frac{\partial u}{\partial x}\right)^2 + \left(\frac{\partial u}{\partial y} + \frac{\partial v}{\partial x}\right)^2\right] + \frac{\sigma B_0^2}{\rho cp\left(1-\gamma t\right)}u^2 \tag{8}$$

In equation (4) Ω_E i.e. the temperature function is formulated following Muhammad *et al.* [35] and Atlas *et al.* [36] may be written as follows:

$$\Omega_E = \frac{\partial^2 T}{\partial t^2} + u\frac{\partial u}{\partial x}\frac{\partial T}{\partial x} + v\frac{\partial v}{\partial y}\frac{\partial T}{\partial y} + 2uv\frac{\partial^2 T}{\partial x \partial y} + u\frac{\partial v}{\partial x}\frac{\partial T}{\partial y} + v\frac{\partial v}{\partial y}\frac{\partial T}{\partial x} + u^2\frac{\partial^2 T}{\partial x^2} + v^2\frac{\partial^2 T}{\partial y^2} + \frac{\partial u}{\partial t}\frac{\partial T}{\partial x}$$
$$+ 2u\frac{\partial^2 T}{\partial x \partial t} + \frac{\partial v}{\partial t}\frac{\partial T}{\partial y} + 2v\frac{\partial^2 T}{\partial y \partial t} \tag{9}$$

To normalize the governing partial differential equation boundary value problem, the following dimensionless local similarity transformations and introduced, following Hayat *et al.* [34]:

$$\eta = \frac{y}{h(t)}, \psi = \sqrt{\frac{av}{1-\gamma t}}x\,f(\eta), u = U_w f'(\eta), v = -\sqrt{\frac{av}{1-\gamma t}}f(\eta), \theta(\eta) = \frac{T-T_f}{T_h-T_f}, \phi = \frac{C-C_f}{C_h-C_f} \right\} \tag{10}$$

Applying these similarity transformations to the governing Eqns. (1)-(5), the mass conservation Eqn. (1) is automatically satisfied and the remaining Eqns. (2)-(5) are converted to the following non-dimensional ordinary differential equations:

$$f''' + f\,f'' - f'\,f'' - \frac{\beta}{2}\left(3f'' + \eta f'''\right) - M^2 f'' - ZBe^{-B\eta} = 0, \tag{11}$$

$$\left(1+R\right)\theta'' + \text{Pr}\left(f\theta' + \frac{\eta}{2}\beta\theta'\right) - \text{Pr}\,\beta_e\left(f\,f'\theta' + f^2\theta'' - \beta\eta f\theta''\right) - \frac{\text{Pr}}{4}\beta_e\beta^2\left(3\eta\theta' + \eta^2\theta''\right)$$
$$+ \frac{\text{Pr}}{2}\beta_e\beta\left(\eta f'\theta' + 3f\theta'\right) + \text{Pr}\,Ec\left[\left(f''\right)^2 + 4\delta^2\left(f'\right)^2 + M^2\left(f'\right)^2\right] = 0 \tag{12}$$

$$\phi'' + Sc\left[f\phi' - \frac{\beta}{2}\eta\phi' - K_c\phi\right] = 0 \quad . \tag{13}$$

Here the dimensionless parameters appearing are defined as:

$$\beta = \frac{\gamma}{a}, B = \frac{\pi h(t)}{b}, M^2 = \frac{\sigma B_0^2}{\rho a}, Z = \frac{\pi j_0 M_0}{8\rho_f U_w^2}x, R = \frac{16 T_h^3 \sigma^*}{3 m^* k}, \Pr = \frac{\mu_f Cp}{k_f}, \beta_e = \frac{S\lambda_E}{(1-\gamma t)},$$

$$Ec = \frac{a^2}{Cp(1-\gamma t)^2(T_f - T_h)}x^2, \quad \delta = \frac{\sqrt{v_f(1-\gamma t)}}{x\sqrt{a}}, \quad Sc = \frac{v}{D_B}, K_c = \frac{K_1(1-\gamma t)}{a} \tag{14}$$

The corresponding boundary conditions (6) are also rendered dimensionless and emerge as:

$$f(\eta) = 0, \quad f'(\eta) = 1, \quad \theta'(\eta) = -B_{i1}(1-\theta(\eta)), \quad \phi'(\eta) = -B_{i2}(1-\phi(\eta)) \quad as\ \eta = 0$$

$$f(\eta) = \frac{\beta}{2}, \quad f'(\eta) = 0, \quad \theta(\eta) = 0, \quad \phi(\eta) = 0 \qquad\qquad as\ \eta = 1 \tag{15}$$

It is observed that for $\beta < 0$, the Riga plates are moving away from each other and for $\beta > 0$ the Riga plates are moving towards each other. In Eqn (15), $B_{i1} = -\frac{h_1}{k}\sqrt{v_f(1-\gamma t)/a}$ denotes Biot number for temperature (thermal Biot number) and $B_{i2} = -\frac{h_2}{k}\sqrt{v_f(1-\gamma t)/a}$ denotes Biot number for concentration (solutal Biot number). The other physical quantities which are of relevance to the current problem are the skin friction coefficient, local Nusselt number and Sherwood numbers which are defined respectively as:

$$C_f = \frac{\tau_w}{\rho_f U_w^2}, \qquad Nu_x = x\frac{q_w}{k_f(T_f - T_h)} + q_r, \qquad Sh_x = x\frac{q_m}{D(C_f - C_h)} \tag{16}$$

Where $\tau_w = \mu_f\left(\frac{\partial u}{\partial y}\right)_{y=h(t)}, \qquad q_w = -k_f\left(\frac{\partial T}{\partial y}\right)_{y=h(t)}, \qquad q_m = -D\left(\frac{\partial C}{\partial y}\right)_{y=h(t)} \quad . \tag{17}$

The appropriate expressions for skin friction, Nusselt number and Sherwood number in dimensionless form are:

$$C_f = \frac{1}{\sqrt{\mathrm{Re}_x}}f''(x), \quad Nu_x = -\frac{(1+R)\sqrt{\mathrm{Re}_x}}{\sqrt{(1-\gamma t)}}\theta'(1), \quad Sh_x = -\sqrt{\mathrm{Re}_x}\phi'(1) \quad . \tag{18}$$

Here $\mathrm{Re}_x = xU_w/v$ is the local Reynolds number.

3 VARIATION OF PARAMETERS METHOD (VPM) SOLUTIONS

The nonlinear ordinary differential boundary value problem described by Eqns. (11)-(13) is an 8th order coupled problem. It is strongly non-linear. Many powerful numerical and analytical methods are available for solving this system. Here the Variation of Parameters Method (VPM) [39] is selected which is an analytical technique free from round off errors, perturbation, linearization or discretization. It uses only the initial conditions which are easier for implementation and reduces the computational work while still maintaining a higher level of accuracy. Recent applications of VPM in viscous flow and heat transfer include Moore and Jones [45] on nonlinear conduction, Zaidi *et al.* [46] on non-Newtonian inclined plane hydrodynamics, Khan *et al.* [47] on thermal

convection flows for fin configurations and Akinshilo and Olofinkua [48] on radiative convection flows. Deploying VPM we consider the general differential equation of the form:

$$Lf(\eta) + Nf(\eta) + Rf(\eta) = g ,$$

(19)

Here L, the higher order (m^{th}) derivative is linear, N denotes the nonlinear terms, R is the remainder terms present in the differential equation and g is the non-homogeneous function. The general iterative solution of VPM takes the form:

$$f_{n+1}(\eta) = f_0(\eta) + \int_0^\eta \lambda(\eta,\xi)\big(-Nf_n(\xi) - Rf_n(\xi) + g(\xi)\big)d\xi ,$$

(20)

Here, $f_0(\eta)$ is the initial function defined as follows:

$$f_0(\eta) = \sum_{r=0}^m K_r \frac{f^r(0)}{r!} ,$$

(21)

The unknown constants i.e. K_r are to be obtained using initial/boundary conditions and $\lambda(\eta,\xi)$ is the multiplier obtained from the Wronskian technique, defined as:

$$\lambda(\eta,\xi) = \sum_{r=0}^m \frac{(-1)^{r-1}\beta^{r-1}\eta^{m-r}}{(r-1)!(m-r)!} = \frac{(\eta-\xi)^{m-1}}{(m-1)!} ,$$

(22)

Following the standard procedure of VPM [39] the appropriate equations for the current dual Riga squeeze film problem may be written as:

$$f_{n+1}(\eta) = f_0(\eta) + \int_0^\eta \left(\frac{\eta^3}{3!} - \frac{\eta^2\xi}{2!} + \frac{\eta\xi^2}{2!} - \frac{\xi^3}{3!}\right) \times$$
$$\left(\frac{\beta}{2}(\xi f_n'''(\xi) + 3f_n''(\xi)) - f_n(\xi)f_n'''(\xi) + f_n'(\xi)f_n''(\xi) + M^2 f_n''(\xi) + ZB\exp(-B\xi)\right)d\xi ,$$

(23)

$$\theta_{n+1}(\eta) = \theta_0(\eta) - \frac{\Pr}{1+R}\int_0^\eta (\eta-\xi) \times \begin{pmatrix} f_n(\xi)\theta_n'(\xi) + \frac{\beta}{2}\xi\theta_n'(\xi) - \beta_e(f_n(\xi)f_n'(\xi)\theta_n'(\xi) + f_n^2(\xi)\theta_n''(\xi) - \\ \beta\xi f_n(\xi)\theta_n''(\xi)) - \frac{\beta_e}{4}\beta^2(3\xi\theta_n'(\xi) + \xi^2\theta_n''(\xi)) + \frac{\beta_e}{2}\beta(\xi f_n'(\xi)\theta_n'(\xi) + \\ 3f_n(\xi)\theta_n'(\xi)) + Ec(f_n''^2(\xi) + (4\delta^2 + M^2)f_n'^2(\xi)) \end{pmatrix} d\xi ,$$

(24)

$$\phi_{n+1}(\eta) = \phi_0(\eta) - \int_0^\eta (\eta-\xi) \times Sc\left(f_n(\xi)\phi_n'(\xi) - \frac{\beta}{2}\xi\phi_n'(\xi) - Kc\phi_n(\xi)\right)d\xi ,$$

(25)

Using an iterative procedure, it is possible then to evaluate $f_1, f_2, f_3, ...\theta_1, \theta_2, \theta_3, ...$ and $\phi_1, \phi_2, \phi_3......$ etc, with the initial conditions:

$$f_0(\eta) = \eta + K_1\frac{\eta^2}{2} + K_2\frac{\eta^3}{3!} ,$$

(26)

$$\theta_0(\eta) = 1 + \left(\frac{1}{Bi_1} + \eta\right)K_3 ,$$

(27)

$$\phi_0(\eta) = 1 + \left(\frac{1}{Bi_2} + \eta \right) K_4 \qquad .$$

(28)

Further the values of $K_i \, 's, i = 1(1)4$ are obtained using the available boundary conditions. Validation of the VPM solutions has been conducted by comparing the solutions with Hayat *et al.* [34] for the non-dissipative case of *Ec = M=0.* Good correlation is achieved as shown in **Table 1**. Confidence in the VPM solutions is therefore justifiably high. In **Table 1** the *skin friction at the upper Riga plate* $f''(1)$ is computed for different values of squeezing parameter (β) and modified Hartmann number (Z). With increasing values of squeezing parameter (β) there is a strong decrease in skin friction. However, with increasing values of modified Hartmann number (Z) there is a weak increase in skin friction.

Table 1: Comparison of HAM Solutions for $f''(1)$ with VPM solutions for different values of *β* and *Z* with *Ec = M = 0.*

β	Z	HAM [34]	VPM (present)
0.1	1.5	1.69635	1.67852
0.3	"	1.08543	1.069613
0.5	"	0.467511	0.435541
"	0.0	0.422159	0.415059
"	1.0	0.452395	0.428714
"	1.5	0.467511	0.435541

4   VPM RESULTS AND DISCUSSION

Thirteen parameters arise in the mathematical model. Here extensive solutions for the impact of *ten* of these parameters (*squeeze parameter β, magnetic field parameter M, modified Hartmann number Z, radiative parameter R, thermal Biot number B_{i1}, concentration Biot number B_{i2}, Eckert number Ec, length parameter δ, Schmidt number Sc and chemical reaction parameter Kc*) on velocity, temperature and concentration profiles are visualized in **Figs. 2-13** *i.e. the other three parameter, namely constant B is constrained always as 10, non-Fourier thermal relaxation parameter βe, is fixed at 0.1 and Prandtl number Pr is prescribed as unity*, **Tables 2-4** further provide solutions for skin friction coefficient, Nusselt number and Sherwood number at the upper Riga plate again with variation in selected parameters.
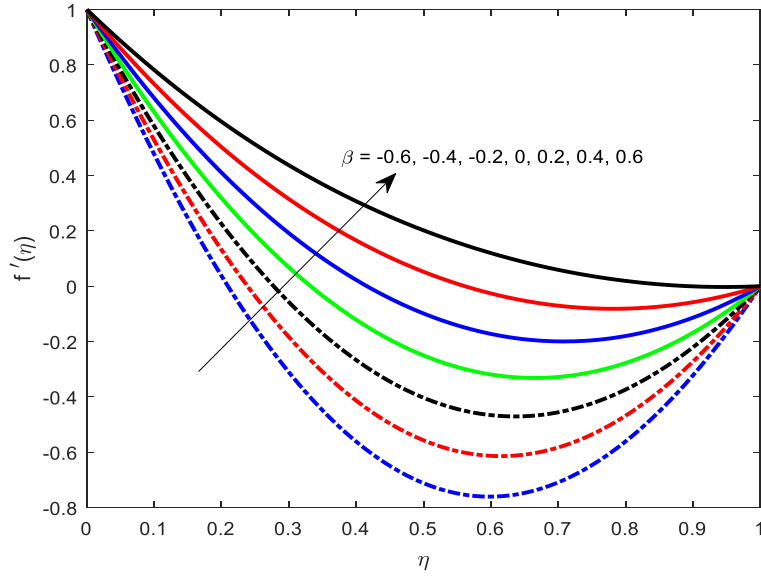
Fig. 2: Effect of squeezing parameter (β) on the velocity profiles for $M=0$, $\beta_e=0.1$, $Sc = 0.5$, $Z=1.5$, $B = 10$, $Pr = 1$, $Ec = 0$, $Kc = 0.2$, $\delta = 0.1$, $R = 0.2$, $B_{i1}= 0.2$, $B_{i2}=0.2$.
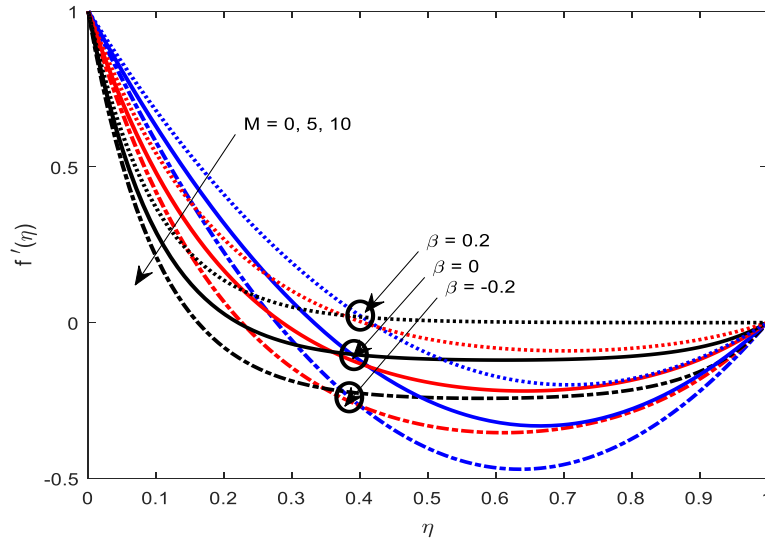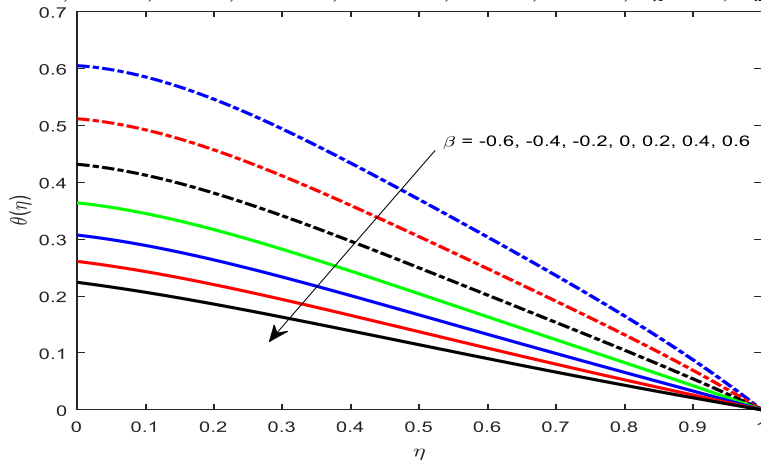

Fig. 3: Effects of magnetic parameter (M), squeezing parameter (β) on the velocity profiles for $\beta_e=0.1$, $Sc = 0.5$, $Z=1.5$, $B = 10$, $Pr = 1$, $Ec = 0.1$, $Kc = 0.2$, $\delta = 0.1$, $R = 0.2$, $B_{i1}= 0.2$, $B_{i2}=0.2$.

Fig. 4: Effect of squeezing parameter (β) on the temperature profiles for $M=0$, $\beta_e=0.1$, $Sc = 0.5$, $Z=1.5$, $B = 10$, $Pr = 1$, $Ec = 0.1$, $Kc = 0.2$, $\delta = 0.1$, $R = 0.2$, $B_{i1}= 0.2$, $B_{i2}=0.2$.
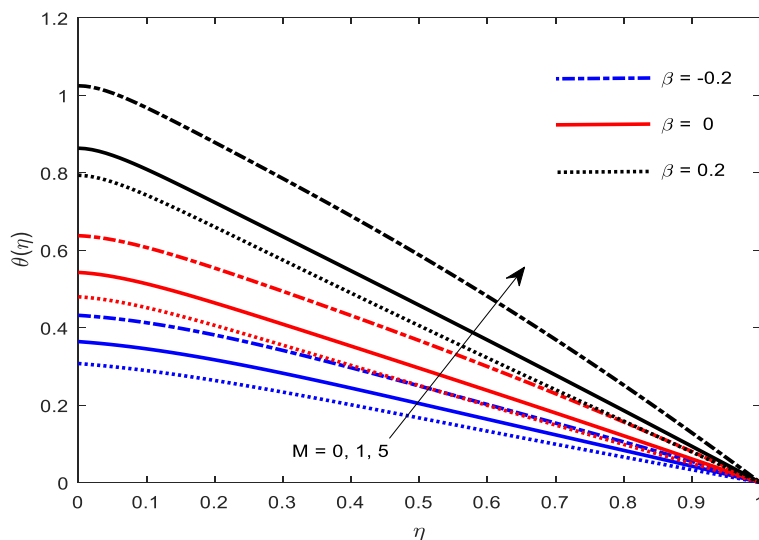
Fig. 5: Effect of magnetic parameter (M) on the temperature profiles for $\beta_e = 0.1$, $Sc = 0.5$, $Z=1.5$, $B = 10$, $Pr = 1$, $Ec = 0.1$, $Kc = 0.2$, $\delta = 0.1$, $R = 0.2$, $B_{i1} = 0.2$, $B_{i2}=0.2$.
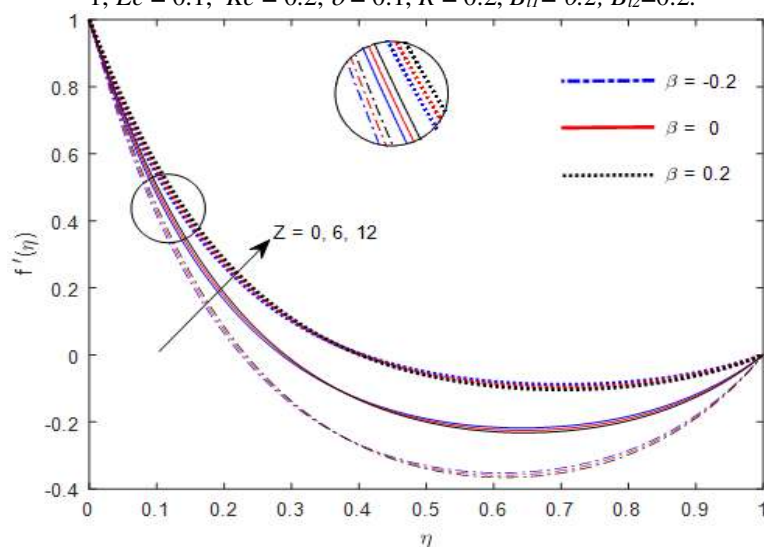

Fig. 6: Effect of modified Hartmann number (Z) on the velocity profiles for $M=5$, $\beta_e = 0.1$, $Sc = 0.5$, $B = 10$, $Pr = 1$, $Ec = 0.1$, $Kc = 0.2$, $\delta = 0.1$, $R = 0.2$, $B_{i1} = 0.2$, $B_{i2}=0.2$.
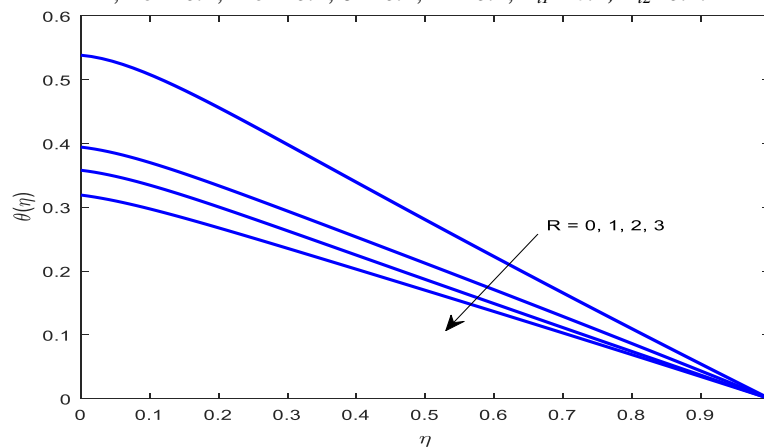

Fig. 7: Effect of thermal radiation parameter (R) on the temperature profiles for $M= 5$, $\beta_e = 0.1$, $\beta = 0.2$, $Sc = 0.5$, $Z=1.5$, $B = 10$, $Pr = 1$, $Ec = 0.1$, $Kc = 0.2$, $\delta = 0.1$, $B_{i1} = 0.2$, $B_{i2}=0.2$.

Fig. 8: Effect of Eckert number (Ec) on the temperature profiles for $M = 5$, $\beta_e = 0.1$, $\beta = 0.2$, $Sc = 0.5$, $Z = 1.5$, $B = 10$, $Pr = 1$, $R = 0.2$, $Kc = 0.2$, $\delta = 0.1$, $B_{i1} = 0.2$, $B_{i2} = 0.2$.
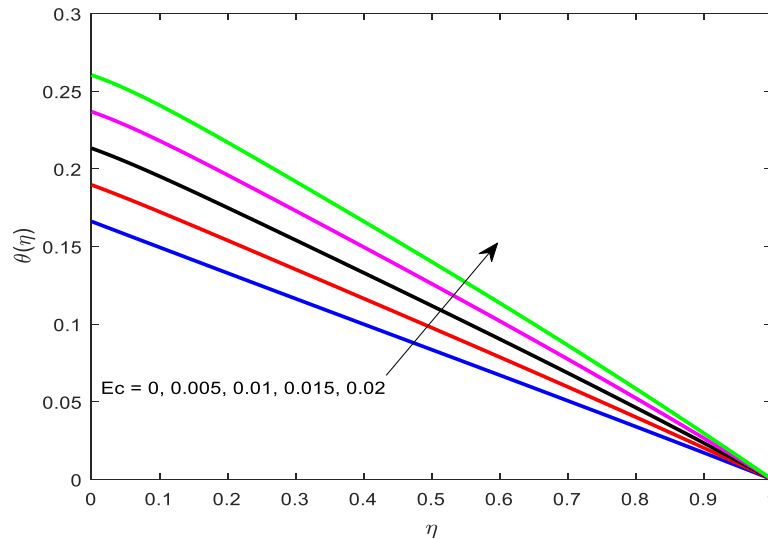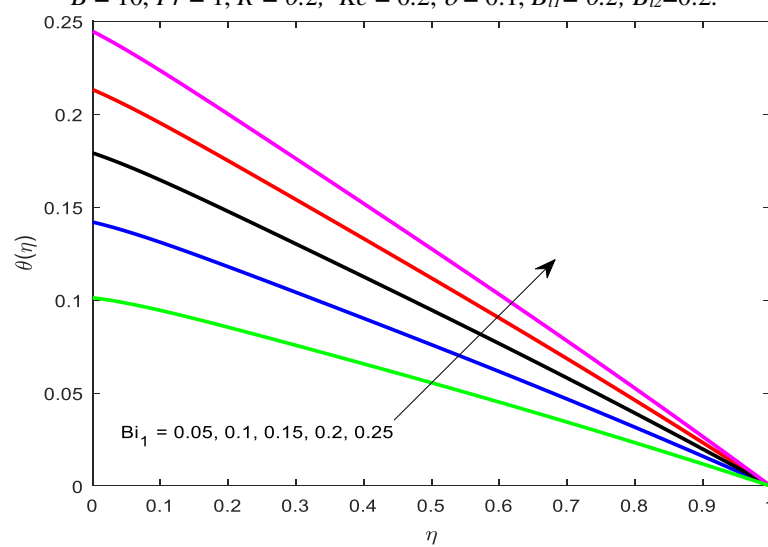

Fig. 9: Effect of thermal Biot number (B_{i1}) on the temperature profiles for $M = 5$, $\beta_e = 0.1$, $\beta = 0.2$, $Sc = 0.5$, $Z = 1.5$, $B = 10$, $Pr = 1$, $R = 0.2$, $Ec = 0.1$, $Kc = 0.2$, $\delta = 0.1$, $B_{i2} = 0.2$.

Fig. 10: Effect of solutal Biot number (B_{i2}) on the concentration profiles for $M = 5$, $\beta_e = 0.1$, $\beta = 0.2$, $Sc = 0.5$, $Z = 1.5$, $B = 10$, $Pr = 1$, $R = 0.2$, $Ec = 0.1$, $Kc = 0.2$, $\delta = 0.1$, $B_{i1} = 0.2$.
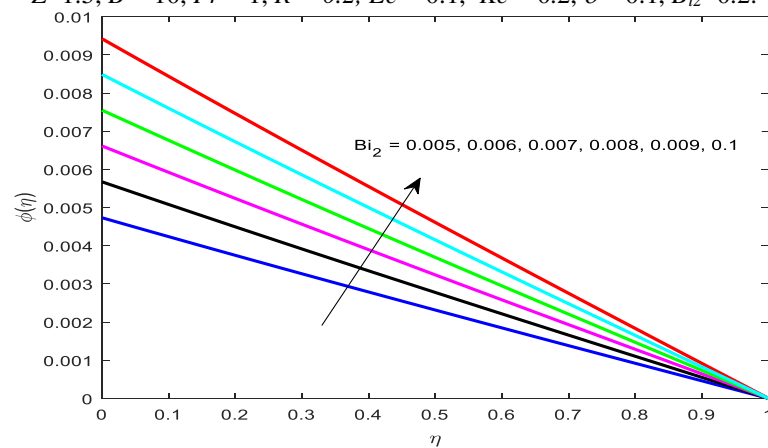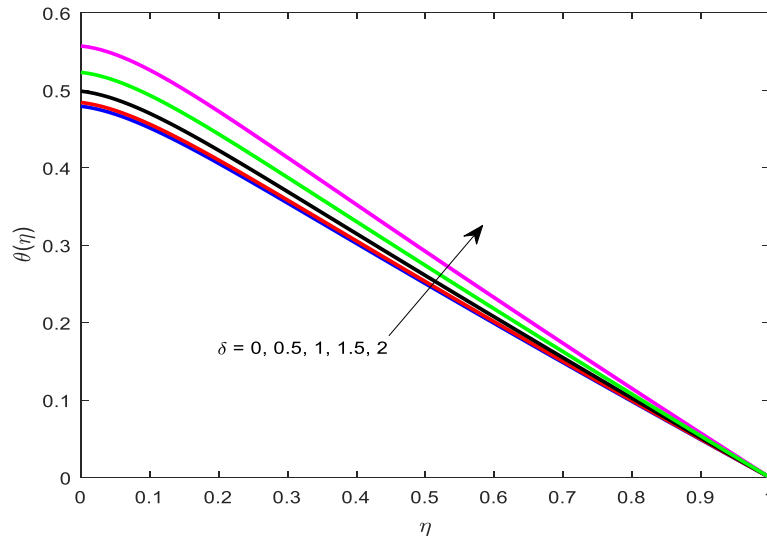
Fig. 11: Effect of length parameter (δ) on the temperature profiles for $M= 5$, $\beta_e =0.1$, $\beta = 0.2$, $Sc = 0.5$, $Z=1.5$, $B = 10$, $Pr = 1$, $R = 0.2$, $Ec = 0.1$, $Kc = 0.2$, $B_{i1}= B_{i2}=0.2$.
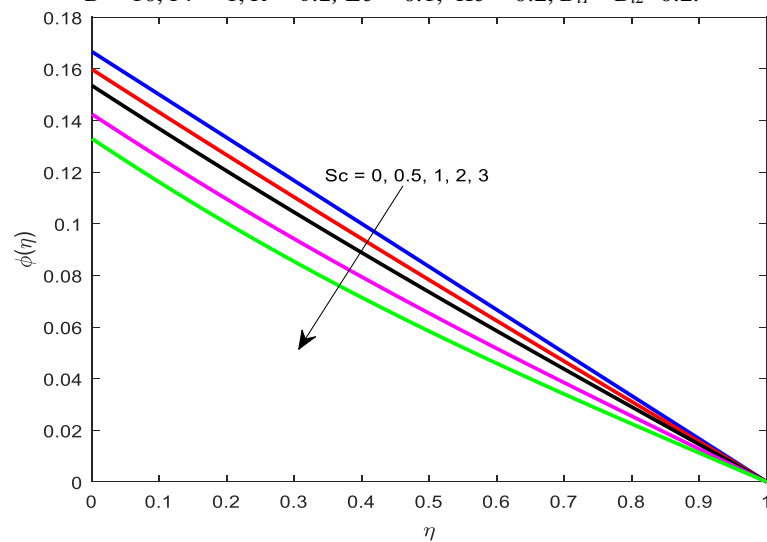
Fig. 12: Effect of Schmidt number (Sc) on the concentration profiles for $M= 5$, $\beta_e =0.1$, $\beta = 0.2$, $Z=1.5$, $B = 10$, $Pr = 1$, $R = 0.2$, $Ec = 0.1$, $Kc = 0.2$, $\delta = 0.1$, $B_{i1}= B_{i2}=0.2$.
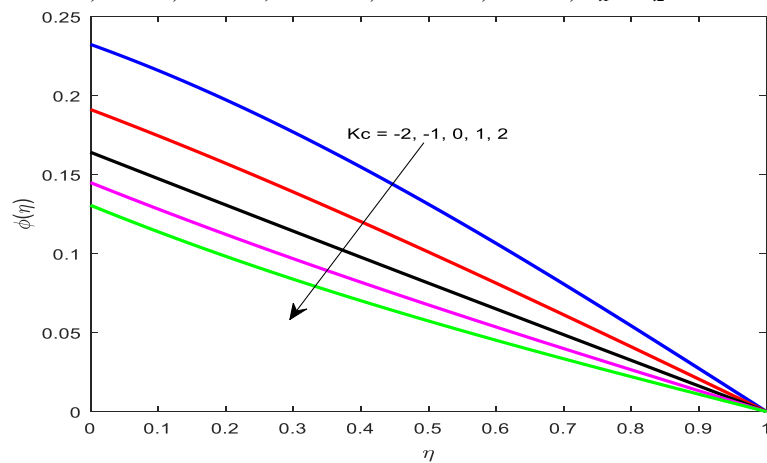

Fig. 13: Effect of chemical reaction parameter (Kc) on the concentration profiles for $M= 5$, $\beta_e =0.1$, $\beta = 0.2$, $Z=1.5$, $B = 10$, $Pr = 1$, $R = 0.2$, $Ec = 0.1$, $Sc = 0.5$, $\delta = 0.1$, $B_{i1}= B_{i2}=0.2$.

Table 2: Values of skin friction coefficient for different values of β, Z, M with β_e =0.1, $B = 10$, $Pr = 1$, $R = 0.2$, $Ec = 0.1$, $Kc = 0.2$, $Sc = 0.5$, $\delta = 0.1$, $B_{i1} = B_{i2} = 0.2$.

β	Z	M	$f''(1)$
0.1	1.5	0	1.67852
0.3			1.069613
0.5			0.435541
	0		0.415059
	1		0.428714
	1.5		0.435541
		1	0.380811
		2	0.228311
		3	0.006099

Table 3: Values of Nusselt number for different values of Ec, δ, R, B_{i1} with $M = 5$, β_e =0.1, $\beta = 0.2$, $B = 10$, $Pr = 1$, $Kc = 0.2$, $Sc = 0.5$, $\delta = 0.1$, B_{i2}=0.2.

Ec	δ	R	Bi_1	$-(1+R)\theta'(1)$
0	0	0.2	0.1	0.135497
0.01				0.152946
0.02				0.170377
	0.1			0.170484
	0.2			0.170808
	0.3			0.171347
		1		0.305357
		2		0.472464
		3		0.63939
		1	0.05	0.120061
			0.1	0.186984
			0.2	0.305357

Table 4: Values of Sherwood number for different values of Sc, Kc and B_{i2} with $M = 5$, $Z= 1.5$, β_e =0.1, $\beta = 0.2$, $B = 10$, $Pr = 1$, $R = 0.2$, $Ec = 0.1$, $\delta = 0.1$, $B_{i1} = 0.2$.

Sc	K_c	Bi_2	$-\phi'(1)$
0.5	0.2	0.2	0.153789
1			0.142203
2			0.122256
0.5	0.3		0.150561
	0.4		0.147442
	0.5		0.144426
		0.3	0.201213
		0.4	0.25045
		0.5	0.29355

Fig. 2 illustrates the evolution of velocity, $f'(\eta)$, across the gap between the Riga plates for variation in squeezing parameter (β) with all other parameters fixed. The prescribed data corresponds to M=0 (applied magnetic field ignored), $\beta_e = 0.1$ (low thermal relaxation time), $Sc = 0.5$ (species has twice the molecular diffusivity as the momentum diffusivity), Z=1.5 (strong magnetization effect from Riga plates), $B = 10$, $Ec = 0$ (viscous dissipation is neglected), $Pr = 1$ (momentum diffusion rate is equivalent to heat diffusion rate), $Kc = 0.2$ (destructive chemical reaction is present), $\delta = 0.1$ (weak length effect), $R = 0.2$ (weak radiative heat transfer relative to conductive heat transfer) and B_{i1}=B_{i2}=0.2 (thermal and solutal Biot numbers are equivalent). Evidently as β increases positively this increases the intensity of the squeezing flow between the Riga plates i.e. they move closer towards each other. However, for increasingly negative values of β the plates increasingly depart from each other. Enhanced squeezing accelerates the flow since it imparts greater inertial influence whereas increased separation of the Riga plates induces deceleration since the viscous effect dominates over inertia. The squeezing parameter is therefore critical in controlling the flow regime between the Riga plates. Similar observations have been reported by Hayat *et al.* [34]. Higher velocities are computed near the upper Riga plate and lower velocities near the lower (stationary) Riga plate. At very high negative squeezing parameter ($\beta = -0.6$) the velocity profile exhibits a strongly parabolic decay from the upper Riga plate to the lower one. As β values become increasingly positive the decay assumes an increasingly linear behavior. There is no applied magnetic field or dissipation effect for this scenario ($M= Ec = 0$).

Fig 3 illustrates the collective influence of magnetic parameter (M) and squeezing parameter (β) on velocity distribution ($f'(\eta)$) across the gap for the case where viscous heating is included (Ec =0.1). Flow acceleration is again apparent for positive β values and flow retardation is induced with negative β values. *The intermediate case of vanishing β implies the upper Riga plate is also stationary i.e. both plates are immobile, and velocities computed fall between the plate squeezing (β =0.2) and plate separating flow ($\beta = -0.2$) case.* With increasing magnetic field parameter, *M*, the Lorentz magnetohydrodynamic body force is enhanced. This leads to significant damping of the flow i.e. a decrease in velocity which is however restricted to the upper channel half space. The re-distribution in momentum results in a corresponding acceleration in the lower channel half space. There is therefore a cross-over in velocity response to external applied magnetic field and this is located near the gap center-line. This is frequently observed in squeezing magnetohydrodynamics as noted by Usha and Sridharan [10]. Again, it is noteworthy that substantial flow control is achieved in the squeezing regime with applied magnetic field, B_o to which *M* is proportional. Furthermore, generally parabolic decays in the velocity profiles from the upper Riga plate to the lower Riga plate are once again observed.

Fig. 4 depicts the impact of squeezing parameter (β) on temperature, $\theta(\eta)$ in the gap between the upper and lower Riga plates i.e. with transverse coordinate, η. It is apparent that the reverse effect is induced as that computed for the velocity field. With increasing positive β values (*stronger squeezing effect*), temperatures are significantly decreased whereas with increasingly negative β values (*enhanced separation of the Riga plates*) temperatures are elevated significantly. Enhanced squeezing therefore curtails thermal diffusion whereas enhanced plate separation encourages it. The regime is therefore heated significantly with a wider gap whereas it is cooled with a narrower gap and this has also been observed in several studies of magnetic squeeze film flows including Muhammad *et al.* [36] and Atlas *et al.* [36]. A linear decrease in temperature is observed from the upper

Riga plate to the lower Riga plate for highest value of positive squeezing parameter. However, with negative values the decay is parabolic especially in the upper half space.

Fig. 5 shows the impact of a variation in magnetic parameter (*M*) and squeezing parameter (*β*) on temperature distribution, $\theta(\eta)$. Increasing magnetic field is found to significantly boost temperatures across the gap. The supplementary work expended in dragging the fluid against the action of the transverse magnetic field, Bo, is dissipated as thermal energy. This heats the fluid in the gap and manifests in a temperature boost. Temperatures are therefore minimized with vanishing magnetic field (*M* =0) and maximized for the case of strongest magnetic field (*M* = 5). Again, with positive *β* values (*stronger squeezing effect*), temperatures are significantly decreased whereas with increasingly negative *β values* (*enhanced separation of the Riga plates*) temperatures are elevated significantly.

Fig. 6 shows the collective influence of modified Hartmann number (Z) and squeezing parameter (*β*) on velocity distribution ($f'(\eta)$) across the gap. Increasing Z exerts the opposite effect to the magnetic parameter, *M*, studied earlier. Larger Z values increase the magnetization between the plates. This effectively serves to accelerate the flow i.e. the opposite effect to the Lorentzian magnetic drag force associated with the applied magnetic field. This feature is unique to Riga plates. The enhanced magnetism between the plates may therefore be successfully utilized to accelerate the flow in the squeezing regime. Velocities are therefore minimized for the case where Z vanishes, and the Riga plates reduce to conventional plates in this scenario. As noted earlier substantially higher magnitudes of velocity are computed at the upper Riga plate compared with the lower Riga plate. At the upper Riga plate (moving) velocity is non-zero whereas at the lower Riga plate velocity vanishes in accordance with the no-slip boundary condition imposed there. Similar observations have been made by Hayat *et al*. [34]. A weak acceleration in the flow is computed with positive squeezing parameter (*β*>0) whereas the opposite behavior i.e. weak deceleration corresponds to the case of a negative squeezing parameter (*β*<0).

Fig. 7 visualizes the impact of radiation parameter, *R* on temperature distribution, $\theta(\eta)$ across the gap. The parameter *R* features in the dimensionless energy conservation Eqn. (12) in the augmented thermal diffusion term. It defines the relative contribution of thermal radiation heat transfer to thermal conduction heat transfer. When *R* = 0 thermal radiation contribution vanishes. When *R* > 1 thermal radiation dominates increasingly over thermal conduction. Although in conventional boundary-layer flows this would lead to energization of the flow and temperature enhancement, in the present regime increasing radiative parameter induces the opposite effect. The suppression of thermal diffusion with squeezing effect is responsible for the decreasing temperatures associated with greater radiation heat flux effect. With radiative flux absent the temperature decay between the upper and lower Riga plates is approximately linear. However, with increasing radiative effect the relationship becomes progressively nonlinear, in particular, in the vicinity of the lower Riga plate.

Figure 8 illustrates the influence of the Eckert number (*Ec*) i.e. dissipation parameter on temperature profiles, $\theta(\eta)$. Eckert number embodies the relative contribution of kinetic energy dissipated to the boundary layer enthalpy difference. For *Ec* = 0 there is no viscous dissipation. As *Ec* increases there is a progressively greater conversion of kinetic energy to heat which results in an elevation in temperatures. *Ec* features in both the viscous heating term, $\mathrm{Pr}\, Ec\, f''^{2}$ and the Joule dissipation term, $\mathrm{Pr}\, Ec\, M^{2} f'^{2}$ both arising in the energy conservation Eqn. (12). With magnetic field imposed as *M* = 5 there is a very strong Joule dissipation effect even with very low

values of *Ec* (associated with incompressible flows). The collective effect is to strongly elevate temperatures across the gap and in all cases the distributions decay from the lower Riga plate ($\eta = 0$) to the upper Riga plate ($\eta = 1$).

Fig. 9 illustrates the influence of thermal Biot number, B_{i1} on temperature profiles, $\theta(\eta)$. This parameter features in the wall boundary conditions at the lower Riga plate in Eqn. (15). $B_{i1} = -\left(h_1 / k\right)\sqrt{v_f\left(1 - \gamma t\right) / a}$ and is a modification of conventional thermal Biot number. When this parameter is smaller than 0.1 this implies physically that the heat conduction inside the lower Riga plate is much faster than the heat convection away from its surface, and temperature gradients are negligible inside of it. This corresponds to the "thermally thin" scenario. When Bi>0.1, heat conduction inside the lower Riga plate is much slower than heat convection away from its surface into the squeezing flow regime, and this is known as the "thermally-thick" scenario. As B_{i1} is increased there is a significant elevation in temperatures across the gap. Greater thermal convection is induced in the flow (i.e. stronger convection currents from the lower Riga plate to the squeezing regime) which becomes heated. The presence of thermal relaxation (β_e >0) also contributes to this.

Fig. 10 shows the response in concentration profiles, $\phi(\eta)$ *to variation in* solutal Biot number, B_{i2} . This parameter $B_{i2} = -\left(h_2 / k\right)\sqrt{v_f\left(1 - \gamma t\right) / a}$ also features in the wall boundary conditions at the lower Riga plate in Eqn. (15). For larger values of this parameter there is a greater contribution in convective mass transfer currents from the lower Riga plate to the squeezing flow regime. This generates an elevation in concentration magnitudes across the gap.

Fig. 11 shows the impact of length parameter, δ on the temperature evolution in the gap. This parameter arises only in the energy conservation Eqn. (15) and is associated with augmenting the dissipation effect. As this parameter increases progressively more kinetic energy is converted to heat and this elevates the temperatures and the effect is most pronounced near the lower Riga plate.

Fig. 12 illustrates the influence of Schmidt number (*Sc*) on concentration profiles between the lower and upper Riga plates. Schmidt number symbolizes the ratio of the momentum to the mass diffusivity in convective mass transfer processes. It effectively quantifies the relative effectiveness of momentum and mass transport by diffusion. Smaller *Sc* values can represent for example hydrogen gas as the species diffusing (*Sc* ~0.2). *Sc* = 1.0 corresponds to both momentum and species diffusion rates being equal. For *Sc* < *1*, species diffusivity exceeds momentum diffusivity and this range is appropriate for low-molecular weight gases (e.g. Hydrogen, Helium) diffusing in air. With increasing *Sc*, there is a strong reduction in concentration magnitudes i.e. mass diffusion is inhibited in the squeezing regime.

Fig. 13 presents the distributions of temperature across the gap with various values of chemical reaction parameter, *Kc*. When *Kc* > 0 this corresponds to the destructive type of homogeneous chemical reaction and it is observed that concentration magnitudes are decreased in the squeezing flow regime since more species is converted via chemical reaction i.e. the original species is reduced. When *Kc* < 0 this implies the constructive type of homogenous reaction and the opposite effect is induced i.e. fewer original species is converted and therefore concentration magnitudes are elevated. Overall for destructive chemical reaction, concentration distributions decrease when the chemical reaction increases. Physically, for a destructive case, with stronger chemical reaction,

greater destruction of the original species takes place. This, in turn, suppresses molecular diffusion of the remaining species which leads to a fall in concentration magnitudes.

Tables 2-4 show the variation in skin friction, Nusselt number and Sherwood number at the upper Riga plate with various parameters. **Table 2** shows that with increasing squeezing parameter (β) and magnetic field parameter (M) there is a strong reduction in skin friction at the upper Riga plate, although the effect is more significant for magnetic field. With increasing modified Hartmann number (Z) the skin friction is conversely increased. **Table 3** reveals that with increasing Eckert number (Ec), length parameter (δ), radiation parameter (R) and thermal Biot number (B_{i1}) there is a consistent elevation in Nusselt number, although the most profound response is induced by thermal Biot number. **Table 4** shows that with increasing Schmidt number (Sc) and chemical reaction parameter (Kc) there is a reduction in Sherwood number (wall mass transfer rate at the upper Riga plate) whereas with increasing solutal Biot number the Sherwood number is substantially enhanced.

5   CONCLUSIONS

A mathematical model has been developed for magnetohydrodynamic squeezing flow, heat and mass transfer between two Riga plates with viscous and Joule heating (Ohmic dissipation). A non-Fourier (Cattaneo-Christov) heat flux model is employed which generalizes the classical Fourier law to incorporate thermal relaxation time. Radiative heat flux is included. The transformed, non-dimensional emerging nonlinear ordinary differential boundary value problem with associated boundary conditions is solved analytically by the variational parameter method (VPM). Validation of the solutions is included for the special case of non-dissipative flow. The current study has shown that:

➢ With increasing Sc, there is a strong reduction in concentration magnitudes i.e. mass diffusion is inhibited in the squeezing regime

➢ When $Kc > 0$ this corresponds to the destructive type of homogeneous chemical reaction and concentration magnitudes are decreased. The opposite behavior is associated with $Kc < 0$ (constructive homogenous chemical reaction).

➢ With increasing thermal Biot number, temperature magnitudes are elevated.

➢ With increasing solutal Biot number, concentration magnitudes are elevated.

➢ With increasing viscous dissipation and Joule dissipation there is a significant increase in temperatures across the gap between the two Riga plates.

➢ Increasing radiative heat transfer results in an overall decrease in temperatures.

➢ Increasing length parameter augments the dissipation effect and results in an increase in temperatures.

➢ Increasing modified Hartmann number corresponds to greater magnetization between the Riga plates and accelerates the flow.

➢ Increasing magnetic field parameter depresses velocities and increases temperatures across the gap.

➢ Increasing positive values of squeezing parameter (*stronger squeezing effect*) increases velocity and reduces temperature whereas the opposite effect is computed increasingly negative values of squeezing parameter (*enhanced separation of the Riga plates*).

➢ With increasing squeezing parameter (β) and magnetic field parameter (M) there is a strong reduction in skin friction at the upper Riga plate.

➢ With increasing modified Hartmann number (Z) the skin friction is enhanced at the upper Riga plate.

➢ With increasing Eckert number (*Ec*), length parameter (*δ*), radiation parameter (*R*) and thermal Biot number (B_{il}) there is a consistent increase in Nusselt number, although the greatest enhancement is induced by thermal Biot number.

➢ With increasing Schmidt number (*Sc*) and chemical reaction parameter (*Kc*) there is a reduction in Sherwood number at the upper Riga plate and the contrary effect is induced with increasing solutal Biot number.

The present study has been restricted to Newtonian fluids and has also neglected a number of thermophysical and other electromagnetic effects. Future investigations may consider two-phase flow and viscoplastic fluid behavior [49], ferrofluid magnetization in rotational systems [50], nano-particle doping [51] and also Hall current and heat generation/absorption effects [52]. Inclusion of these phenomena will serve to generalize the present Riga plate model further and may shed more light on the flows intrinsic to smart sensor systems. The variational parameter method (VPM) appears to hold significant promise in simulating such multi-physical problems in electromagnetic sensor technologies.

DECLARATIONS:

REFERENCES

[1] Moore, D.F.: A review of squeeze films. Wear. 8(4), 245-263 (1965).

[2] Bouzidane, A., Thomas, M.: Nonlinear dynamic behavior of a flexible shaft supported by smart hydrostatic squeeze film dampers. ASME J. Tribol., 135(3), 031701-031701-9 (2013).

[3] Shamshuddin, MD., Mishra, S. R., Kadir, A., Bég, O. Anwar: Unsteady chemo-tribological squeezing flow of magnetized bioconvection lubricants: numerical study. J. Nanofluids., 8(2), 407-419 (2019).

[4] Cookson, R.A., Kossa, S.S.: The effectiveness of squeeze-film damper bearings supporting flexible rotors without a centralising spring. Int. J. Mech. Sci. 22, 313-324 (1980).

[5] Marrero, V., Borca-Tasciuc, D.A., Tichy, J.: On squeeze film damping in microsystems. ASME J. Tribol. 132(3), 031701-031701-6 (2010).

[6] Yousif, A.E., Al-allaq, A.A.: The hydrodynamic squeeze film lubrication of the ankle joint. Int. J. Mech. Eng. Applic. 1(2), 34–42 (2013).

[7] Hlaváček, M.: Squeeze-film lubrication of the human ankle joint subjected to the cyclic loading encountered in walking. ASME J. Tribol. 127(1), 141-148 (2005).

[8] Bujurke, N.M., Kudenatti, R.B., Awati, V.B.: Effect of surface roughness on squeeze film poroelastic bearings with special reference to synovial joints. Math. Biosci. 209, 76–89 (2007).

[9] Wang, J., Feng, N., Meng, G., Hahn, E.J.: Vibration control of rotor by squeeze film damper with magnetorheological fluid, J. Intelligent Material Systems and Structures. 17, 353-357 (2006).

[10] Usha, R., Sridharan, R.: Effect of mass transfer on a similar flow in the magnetohydrodynamic squeeze film. ASME J. Appl. Mech. 64 (1), 240-243 (1997).

[11] Vadher, P.A., Deheri, G.M., Patel, R.M.: Performance of hydromagnetic squeeze films between conducting porous rough conical plates. Meccanica. 45, 767–783 (2010).

[12] Shrimpi, M.E., Deheri, G.M.: A study on the performance of a magnetic fluid-based squeeze film in curved porous rotating rough annular plates and deformation effect. Tribol. Int. 47, 90-99 (2012).

[13] Usha, R., Vimala, P.: Magnetohydrodynamic squeeze film characteristics between parallel circular plates containing a single central air bubble in the inertial flow regime. ASME J. Appl. Mech. 66(4), 1021-1023 (1999).

[14] Zueco, J., Bég, O.Anwar: Network numerical analysis of hydromagnetic squeeze film flow dynamics between two parallel rotating disks with induced magnetic field effects. Tribol. Int., 43, 532-543 (2010).

[15] Kumar, K.G., Gireesha, B.J., Krishnamurthy, M.R., Rudraswamy, N.G.: An unsteady squeezed flow of a tangent hyperbolic fluid over a sensor surface in the presence of variable thermal conductivity. Results Phys. 7, 3031-3036 (2017).

[16] Gailitis, A., Lielausis, O.: On a possibility to reduce the hydrodynamics resistance of a plate in an electrolyte. Appl. Magnet. Rep. Phys. Inst. 12, 143–146 (1961).

[17] Ahmad, A., Asghar, S., Afzal, S.: Flow of a nanofluid past a Riga plate. J. Magn. Magn. Mater. 402, 44–48 (2016).

[18] Anjum, A.: Physical aspects of heat generation/absorption in the second-grade fluid flow due to Riga plate: Application of Cattaneo-Christov approach. Results Phys. 9, (2018). DOI: 10.1016/j.rinp.2018.03.024.

[19] Hayat, T., Ullah, I., Alsaedi, A., Ahmad, B.: Simultaneous effects of nonlinear mixed convection and radiative flow due to Riga-plate with double stratification. ASME J. Heat Transfer. 140(10), 102008 (2018). DOI:10.1115/1.4039994.

[20] Mao, J., Aleksandrova, S., Molokov, S.: Joule heating in magnetohydrodynamic flows in channels with thin conducting walls. Int. J Heat and Mass Transfer. 51, 4392–4399 (2008).

[21] El-Amin, M.F.: Combined effect of viscous dissipation and Joule heating on MHD forced convection over a non-isothermal horizontal cylinder embedded in a fluid saturated porous medium. J. Magn. Magn. Mater. 263, 337-343 (2003).

[22] Bég, O.Anwar, Zueco, J., Takhar, H.S.: Unsteady magnetohydrodynamic Hartmann–Couette flow and heat transfer in a Darcian channel with Hall current, ionslip, viscous and Joule heating effects: Network numerical solutions. Commun. Nonlinear Sci. Numer. Simult. 14, 1082-1097 (2009).

[23] Srinivasacharya, D., Jagadeeshwar, P.: MHD flow with Hall current and Joule heating effects over an exponentially stretching sheet. Nonlinear Eng. Modell. Applic. 6 (2), 101-114 (2017).

[24] Aurangzaib., S. Shafie.: Thermal diffusion and diffusion thermo effects on unsteady MHD free convection flow over a stretching surface considering Joule heating and viscous dissipation with thermal stratification, chemical reaction and Hall current. J. Franklin Institute, 351, 1268–1287 (2014).

[25] Tripathi, D., Sharma, A., Bég, O.Anwar: Electrothermal transport of nanofluids via peristaltic pumping in a finite micro-channel: effects of Joule heating and Helmholtz-Smoluchowski velocity. Int. J. Heat Mass Transfer, 111, 138–149 (2017).

[26] Golsefid, S.S.M., Amanifard, N., Deylami, H.M., Dolati, F.: Numerical and experimental study on EHD heat transfer enhancement with Joule heating effect through a rectangular enclosure. Appl. Therm. Eng., 123, 689-698 (2017).

[27] Shamshuddin, MD., Mishra, S.R., Bég, O.Anwar, Kadir, A.: Unsteady reactive magnetic radiative micropolar flow, heat and mass transfer from an inclined plate with Joule heating: a model for magnetic polymer processing. Proc. IMechE- Part C. – Mech. Eng. Sci. (2018) (16 pages). DOI: 10.1177/0954406218768837.

[28] Hussain, A., Malik, M.Y., Salahuddin, T., Bilal, S., Awais, M.: Combined effects of viscous dissipation and Joule heating on MHD Sisko nanofluid over a stretching cylinder. J. Mol. Liq., 231, 341-352 (2017).

[29] Bég, O.Anwar, Gaffar, S.A., Prasad, V.R., Uddin, M.J.: Computational solutions for non-isothermal, nonlinear magnetoconvection in porous media with Hall/ionslip currents and Ohmic dissipation. Eng. Sci. Tech-An Int. J. 19, 377-394 (2016).

[30] Sucharitha, G., Lakshminarayana, P., Sandeep, N.: Joule heating and wall flexibility effects on the peristaltic flow of magnetohydrodynamic nanofluid. Int. J. Mech. Sci. 131/132, 52-62 (2017).

[31] Ahmad, S., Farooq, M., Anjum, A., Javed, M., Malik, M.Y., Alshomrani, A.S.: Diffusive species in MHD squeezed fluid flow through non-Darcy porous medium with viscous dissipation and Joule heating. J. Magnetics. 23(2), 323-332 (2018).

[32] Ghadikolaei, S.S., Hosseinzadeh, Kh., Ganji, D.D.: Analysis of unsteady MHD Eyring-Powell squeezing flow in stretching channel with considering thermal radiation and Joule heating effect using AGM. Case Studies in Thermal Eng. 10, 579-594 (2017).

[33] Christov, C.I.: On frame indifferent formulation of the Maxwell-Cattaneo model of finite speed heat conduction. Mech. Res. Commun. 36, 481–486 (2009).

[34] Hayat, T., Khan, M., Imtiaz, M., Alsaedi, A.: Squeezing flow past a Riga plate with chemical reaction and convective conditions. J. Mol. Liq., 225, 569-576 (2017).

[35] Muhammad, N., Nadeem, S., Mustafa, T.: Squeezed flow of a nanofluid with Cattaneo- Christov heat and mass fluxes. Res. Phys. 7, 862-869 (2017).

[36] Atlas, M., Hussain, S., Sagheer, M.: Entropy generation and squeezing flow past a Riga plate with Cattaneo-Christov heat flux. Bulletin of the Polish Academy of Sciences Technical Sciences. 66(3), 291-300 (2018).

[37] Shamshuddin, MD., Mishra, S.R., Bég, O.Anwar, Kadir, A.: Numerical study of heat transfer and viscous flow in a dual rotating extendable disk system with a non-Fourier heat flux model. Heat Transfer - Asian Research. (2018). https://doi.org/10.1002/htj.21392

[38] Rashid, M., Rana, S., Bég, O.Anwar, Kadir, A.: Numerical study of chemical reaction effects in magnetohydrodynamic Oldroyd-B oblique stagnation flow with a non-Fourier heat flux model. J. Brazilian Soc. Mech Sci. Eng. 40, 526 (2018). https://doi.org/10.1007/s40430-018-1446-4.

[39] Ma, W.X., You, Y.: Solving the Korteweg-de Vries equation by its bilinear form: Wronskian solutions. Trans American Math Soc. 357, 1753-1778 (2014).

[40] Tian, Z.Z., Chen, F., Wang, D.M.: Influence of interface deformation on transmittable torque of disk-type magnetorheological clutch. J. Intelligent Material Systems and Structures. 26, 414-424 (2016).

[41] Kumar, L et al.: MEMS oscillating squeeze-film pressure sensor with optoelectronic feedback. J. Micromech. Microeng. 25(4), 045011 (2015). https://doi.org/10.1088/0960-1317/25/4/045011.

[42] Khaled, R.A., Vafai, K.: Hydromagnetic squeezed flow and heat transfer over a sensor surface. Int. J Eng. Sci. 42, 509-519 (2004).

[43] Rizwan Ul Haq., Nadeem, S., Khan, Z.H., Noor, N.F.M.: MHD squeezed flow of water functionalized metallic nanoparticles over a sensor surface. Physica E: Low-dimensional Systems and Nanostructures, 73, 45-53 (2015).

[44] Modest, M.F.: Radiation Heat Transfer, MacGraw-Hill, NY (1993).

[45] Moore, T.J., M.R. Jones, M.R.: Solving nonlinear heat transfer problems using variation of parameters. Int. J Thermal Sci. 93, 29-35 (2015).

[46] Zaidi, Z.A., Jan, S.U., Ahmed, N., Khan, U., Mohyud-Din, S.T.: Variation of parameters method for thin film flow of a third-grade fluid down an inclined plane. Ital. J. Pure Appl. Math. 31, 161–168 (2013).

[47] Khan, S.I., Khan, U., Ahmad, N., Mohyud-Din, S.T.: Variation of parameters method for heat diffusion and heat convection equations. Int. J. Appl. Comput. Math. 3, 185–193 (2017).

[48] Akinshilo, A.T., Olofinkua, J.O.: Variation of Parameters method for thermal analysis of straight convective-radiative fins with temperature dependent thermal conductivity. J. Comput. Appl. Mech. 49, 125-132 (2018).

[49] Mahanthesh, B., Gireesha, B.J.: Scrutinization of thermal radiation, viscous dissipation and Joule heating effects on Marangoni convective two-phase flow of Casson fluid with fluid particle suspension. Results in Physics. 8, 869-878 (2018).

[50] Sampath Kumar, P.B. Gireesha, B.J., Mahanthesh, B., Gorla, R.S.R.: Radiative nonlinear 3D flow of ferrofluid with Joule heating, convective condition and Coriolis force. Therm. Sci. Eng. Prog. 3, 88-94 (2017).

[51] Mahanthesh, B., Gireesha, B.J., Prasannakumara, B.C., Shashikumar, N.S.: Marangoni convection radiative flow of dusty nanoliquid with exponential space dependent heat source. Nuclear Eng. Tech. 49(8), 1660-1668 (2017).

[52] Gireesha, B.J., Mahanthesh, B., Gorla, R.S.R., Manjunatha, P.T.: Thermal radiation and Hall effects on boundary layer flow past a non-isothermal stretching surface embedded in porous medium with non-uniform heat source/sink and fluid-particle suspension. Heat and Mass Transfer. 52(4), 897-911(2016).